RSC Advances

ROYAL SOCIETY OF CHEMISTRY

www.rsc.org/advances

Journal Name

ARTICLE

Ti-doped $SrFeO_3$ nanostructured electrodes for Symmetric Solid Oxide Fuel Cells

Received 00th January 20xx,
Accepted 00th January 20xx

DOI: 10.1039/x0xx00000x

www.rsc.org/

L. dos Santos-Gómez[a], J. M. Porras-Vázquez[a], E. R. Losilla[a], D. Marrero-López[b,*]

Nanostructured electrodes of $Sr_{0.98}Fe_{1-x}Ti_xO_{3-\delta}$ are evaluated as both cathode and anode for Solid Oxide Fuel Cells. The electrodes are prepared by a low-cost and simple procedure based on spray-pyrolysis deposition on a porous $Ce_{0.8}Gd_{0.2}O_{1.9}$ (CGO) layer. A homogenous coating layer of electrode catalyst nanoparticles is formed on the CGO backbone surface in a single deposition-firing step. $Sr_{0.98}Fe_{0.8}Ti_{0.2}O_{3-\delta}$ ($SFT_{0.2}$) exhibits high efficiency operating as both cathode and anode with polarization resistance values of 0.1 Ωcm^2 in air and 0.07 Ωcm^2 in humidified H_2 at 700 ºC. An electrolyte supported cell with 300 µm thick $La_{0.9}Sr_{0.1}Ga_{0.8}Mg_{0.2}O_{3-\delta}$ electrolyte and $SFT_{0.2}$ symmetric electrodes shows maximum power densities of 700 and 140 $mWcm^{-2}$ at 800 and 600 ºC, respectively.

Introduction

Solid Oxide Fuel Cells (SOFCs) are considered as one of the most efficient and cleanest technologies for power generation.[1] However, the high operating temperature and manufacturing cost have limited their large-scale commercialization. A typical single SOFC is composed of three ceramic components; a dense electrolyte sandwiched between a porous cathode and anode made of different materials, which are exposed to the oxidant and fuel gases respectively.[2] This traditional configuration might be replaced by a new approach, where the same electrode materials are used as both cathode and anode to obtain a symmetrical solid oxide fuel cell (SSOFC).[3,4] SSOFCs have attracted great attention in last few years because they exhibit several advantages compared to traditional SOFCs.[5,6] For example, the mechanical and chemical compatibility between the electrolyte and electrodes is improved, since the number of different cell components and interfaces are reduced. The production of SSOFC is easier, because of the electrolyte and electrodes may be assembled in just one thermal process, reducing fabrication time and costs. However, the most important advantage of SSOFC is the possibility to eliminate sulphur and carbon deposits in the anode by simply reversing the gas flow to oxidize these species and recover the initial performance.

The electrode materials for SSOFC were initially limited to those structurally stable under both reducing and oxidizing conditions, such as $La_{0.75}Sr_{0.25}Cr_{0.5}Mn_{0.5}O_{3-\delta}$, $La_{0.7}Ca_{0.3}CrO_{3-\delta}$, $La_{0.8}Sr_{0.2}Sc_{0.2}Mn_{0.8}O_{3-\delta}$, $La_{0.6}Sr_{0.4}Fe_{0.9}Sc_{0.1}O_{3-\delta}$, $Sr_2Fe_{1.5}Mo_{0.5}O_{6-\delta}$, $La_4Sr_8Ti_{12-x}Fe_xO_{38-\delta}$, $La_{0.5}Sr_{0.5}Ti_{0.5}O_{3-\delta}$ and $SrCo_{1-x}MoO_{3-\delta}$.[3-17] Materials, which undergo a phase transformation on reduction, have also been investigated, such as $Ba_{0.5}Sr_{0.5}Fe_{0.8}Cu_{0.1}Ti_{0.1}O_{3-\delta}$, $La_{0.6}Sr_{0.4}Co_{0.8}Fe_{0.2}O_{3-\delta}$ and La_2NiO_4.[18-22] Although, strictly, these compounds should not be considered as symmetric electrodes because the phase composition under oxidizing and reducing atmospheres is different. These materials are usually mixed compounds when operate as anode, containing metal particles that improve the performance. Nevertheless, the stability of these electrodes after successive oxidizing/reducing cycles of operation is questionable, especially at moderate temperatures where the reversibility of the phase transformation was not studied.

Among the redox stable materials, $SrFeO_{3-\delta}$ may be doped with different transition metals, possessing better redox stability than iron, such as Ti^{4+}, Si^{4+}, Zr^{4+}, Mo^{6+} and W^{6+}, leading to the stabilization of the cubic polymorph in a wide range of temperatures and oxygen partial pressures.[23-27] These dopants also suppress the phase transition to the brownmillerite structure with ordered oxygen vacancies and lower mixed ionic-electronic conductivity. Ti-doped $SrFeO_{3-\delta}$ is among the most promising materials, with polarization resistance values of 0.5 Ωcm^2 in 5% H_2-Ar and 0.1 Ωcm^2 in air at 800 ºC.[24]

On the other hand, the performance of SSOFCs is usually lower compared to the traditional SOFCs due to the lower efficiency of the symmetric electrodes, especially operating as anode. The optimization of the electrode microstructure is a possibility to improve the electrode properties. In this context, the preparation of nanostructured electrodes by infiltration into a porous electrolyte scaffold is an effective strategy to increase the triple-phase-boundary (TPB) sites and the electrode performance.[28-31] However, this method is tedious and requires multiple impregnation-calcination steps to achieve sufficient conductivity and stability of the electrodes.

Spray-pyrolysis deposition is another simple and cost-effective technique to obtain nanocrystalline electrodes for SOFCs. This method has been widely used to obtain different electrodes: $La_{0.8}Sr_{0.2}MnO_{3-\delta}$,[32-34] $La_{0.6}Sr_{0.4}Co_{1-x}Fe_xO_{3-\delta}$,[35-39] $Sm_{0.5}Sr_{0.5}O_{3-\delta}$,[40] $La_4Ni_3O_{10-\delta}$,[41] and Ni-CGO.[42-43]

[a] Universidad de Málaga, Departamento de Química Inorgánica, 29071-Málaga, Spain.
[b] Universidad de Málaga, Departamento de Física Aplicada I, Laboratorio de Materiales y Superficie, 29071-Málaga, Spain.

† Footnotes relating to the title and/or authors should appear here.
Electronic Supplementary Information (ESI) available: [XRD patterns of the materials prepared from different precursors; Unit cell volume variation; Rietveld plot; SEM micrograph of the electrode prepared by freeze-drying precursor; cross-sectional micrograph of the symmetrical fuel cell]. See DOI: 10.1039/x0xx00000x

In a previous study, $La_{0.8}Sr_{0.2}MnO_{3-\delta}$ cathode was deposited by spray-pyrolysis on a porous electrolyte scaffold to extend the triple-phase boundary, resulting in a substantial improve of the performance.[44] This procedure is easily adaptable to industrial scale, allowing the deposition of different electrodes in a short and single thermal process and with better reproducibility compared to the classical wet-infiltration process.

In this work, this alternative method is used to prepare Ti-doped $SrFeO_{3-\delta}$ symmetric electrodes. The structure, microstructure and electrochemical properties of these nanostructured electrodes are investigated and compared with submicrometric electrodes obtained by freeze-drying method and deposited at high temperatures on the electrolyte.

2. Experimental Section

2.1. Materials preparation.

The electrolyte used in this study, $La_{0.9}Sr_{0.1}Ga_{0.8}Mg_{0.2}O_{3-\delta}$ (LSGM), was prepared from freeze-dried precursor powders as described elsewhere.[45] The powders were pressed into pellets of 13 and 1 mm of diameter and thickness, respectively and then sintered at 1400 ºC for 4 h. Porous $Ce_{0.8}Gd_{0.2}O_{1.9}$ (CGO, Rhodia) backbones were deposited symmetrically on both faces of the LSGM electrolyte. For this purpose, the powders were mixed with a binder material Decoflux™ (WB41, Zschimmer and Schwarz). The resulting ink was screen-printed onto both faces of the LSGM pellets and sintered at 1100 ºC for 1 h to ensure adequate adherence. After that $Sr_{0.98}Fe_{1-x}Ti_xO_{3-\delta}$ (x=0-0.8) electrodes (SFT_x) were deposited on CGO backbone by spray-pyrolysis (SP). The deposition temperature was low enough to allow the incorporation of the catalyst electrode solution inside the porous CGO backbone.

The undoped compound, $SrFeO_{3-\delta}$, was firstly prepared from different precursor solutions to study the phase formation: i) an aqueous solution based on metal nitrates, where $Sr(NO_3)_2$ (Aldrich, 98%) and $Fe(NO_3)_3{\cdot}9H_2O$ (Aldrich, 99.99%) were dissolved in water with a concentration of 0.025 M; ii) an aqueous solution of acetates, where $Sr(CH_3CO_2)_2$ and $Fe(CH_3CO_2)_3$ (Alfa-Aesar, +99%) were dissolved in water with concentration of 0.025 M; and iii) an aqueous nitrate solution containing ethylenediamine-tetraacetic acid (EDTA) as a complexing agent in a 1:0.5 ligand:metal molar ratio.

The titanium solution was prepared separately from $Ti[OCH(CH_3)_2]_4$ (Aldrich, 97%), which was weighed on absolute ethanol and then EDTA solution was added as complexing agent. This solution was heated with continuous stirring to remove the ethanol. Finally, the different cation solutions were mixed in stoichiometric quantities.

The resulting solutions were sprayed onto amorphous quartz substrates and symmetrically on both faces of the CGO backbone to study the structure of the deposited electrodes and the electrical properties, respectively. The spraying process was made through a circular shadow mask by using a homemade spray-pyrolysis setup equipped with a syringe pump, motion and temperature controllers. The substrates were heated on an aluminium plate at 250 ºC and moved continuously at a constant speed under the spray-nozzle to obtain homogeneous electrode deposition. The solutions were atomized by using compressed air as carrier gas at a pressure of 2 atm. The deposition time, solution flow rate, and nozzle to substrate distance were 60 min, 20 mL/h and 25 cm, respectively.[44]

The films were thermally treated in a furnace between 650 and 800 ºC in air for 2 h in order to crystallize the electrodes and to study the phase evolution with the temperature. Only those samples prepared with EDTA were single-phase materials as discussed in the next section. For this reason, Ti-containing samples were prepared from (iii) nitrate salts and EDTA.

Submicrometric powders of $SrFe_{0.8}Ti_{0.2}O_{3-\delta}$ were also prepared by the freeze-drying method (FD) as detailed in the previous work.[24] A composite of 50 wt% $SFT_{0.2}$-CGO was prepared by mixing the powders in a planetary ball-milling, followed by screen-printing on LSGM pellets, and finally sintered at 1100 ºC for 1 h.

2.2. Materials characterization.

The structure of the electrodes was investigated by X-ray powder diffraction (XRD) with a PANalytical X´Pert diffractometer using $CuK_{\alpha 1}$ radiation. The phase identification and analysis were performed with X´Pert HighScore and GSAS suite software.[46,47]

The morphology of the electrodes was observed by Field Emission SEM (FEI, Helios Nanolab 650) combined with energy dispersive X-ray spectroscopy (EDX).

Polarization resistance of the electrodes in symmetrical cells was determined by impedance spectroscopy (Solartron 1260) in the frequency range 0.01-10^6 Hz, with an ac voltage of 25 mV. Pt paste and meshes were used as current collectors. Impedance spectra were acquired by flowing three different gases: air, humidified 5% H_2-Ar and pure H_2 (3% H_2O). Measurements were taken on cooling between 750 and 300 ºC with a dwell time of 30 min at each temperature. Data was also acquired as a function of the oxygen partial pressure (pO_2) to determine the different rate limiting steps on the cathode polarization by using an electrochemical cell equipped with an YSZ oxygen pump and sensor. The data were fitted to equivalent circuit models with ZView software.[48]

Single fuel cells were fabricated using a 300 µm thick LSGM electrolyte with $Sr_{0.98}Fe_{0.8}Ti_{0.2}O_{3-\delta}$ symmetric electrodes; deposited by spray-pyrolysis on the CGO backbone, following the procedure described above. The cell was sealed to the electrochemical setup using a ceramic-based material (Ceramabond 668, Aremco). Impedance spectra and current-voltage curves were collected with a VSP multichannel potentiostat/galvanostat/FRA (Bio-Logic) between 600 and 800 ºC using humidified H_2 (3% H_2O) as fuel and static air as oxidant. The measurements were performed after reducing the anode material for 1 h in 5% H_2-Ar at 750 ºC.

3. Results and Discussion

3.1. Structure and microstructure of the electrodes.

$Sr_{0.98}Fe_{1-x}Ti_xO_{3-\delta}$ (x = 0, 0.2, 0.4 and 0.8) series was prepared by spray-pyrolysis on amorphous quartz substrates to test the purity of the samples. The materials were slightly Sr-deficient to avoid Sr segregation, which have a detrimental impact on the properties and stability of the electrodes as previously reported. [49]

XRD patterns for the parent compound, $SrFeO_{3-\delta}$, obtained from different cation solutions and calcined at 650 ºC, are given as supplementary information in Fig. S1. The film prepared from a nitrate based solution (without EDTA) shows the presence of $SrFeO_{3-\delta}$ as main crystalline phase, besides of impurities of $SrCO_3$ and other unidentified phases. The film prepared from the acetate solution is a mixture of phases containing $SrFeO_{3-\delta}$ and $SrFe_{12}O_{19}$ (ICSD 16158). In contrast, the solution with nitrates and EDTA leads to a single $SrFeO_3$-related phase.

These films were also annealed at 800 ºC and compositional changes were not observed.

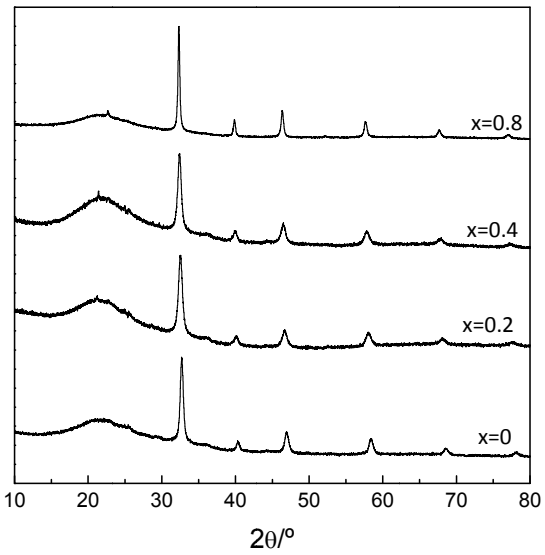

Fig. 1. XRD patterns for $Sr_{0.98}Fe_{1-x}Ti_xO_{3-\delta}$ films deposited by spray-pyrolysis on amorphous quartz substrates after calcining at 650 ºC for 2 h.

It has to be mentioned that $SrFeO_{3-\delta}$ exhibits different polymorphs; brownmillerite and perovskite-type with cubic/orthorhombic symmetric, possessing the cubic symmetry the best electrical properties for SOFC applications.[50,51] The stabilization of these polymorphs at room temperature is directly related to the oxygen content, oxygen vacancy distribution and iron oxidation state in the lattice. Thus, the different polymorphs may be obtained by varying the synthesis procedure, temperature, oxygen partial pressure and doping strategy. In this work, the parent compound $Sr_{0.98}FeO_{3-\delta}$, crystallizes with a cubic symmetry because peak splitting is not observed in the XRD patterns (Fig. 1). In contrast, the same composition prepared by freeze-drying shows peak splitting, suggesting the stabilization of the orthorhombic perovskite structure.[24] The different behavior is attributed to the synthesis method used, temperature and crystallite size, i.e. 20 nm for SP films at 650 ºC and 100 nm for FD powders at 800 ºC. The cubic symmetry is also stabilized at high temperatures and low oxygen partial pressures through Ti-doping, because Ti^{4+} is not as prone to be reduced as Fe^{4+}. This can be clearly observed in Figure 1, where all Ti-doped samples crystallize with cubic symmetry. Note also that previous studies reported that Ti-doped $SrFeO_{3-\delta}$ exhibit sufficient redox stability to be used as SOFC anode up to 800 ºC.[24,52]

The cell volume for films prepared by spray-pyrolysis and powders from freeze-drying was determined by the Rietveld method (Fig. S2, supplementary information). The cell volume increases with Ti-content from 57.90 $Å^3$ for x=0, to 59.94 $Å^3$ for x=0.8 due to larger ionic radius of Ti^{4+} (0.605 Å) compared to that of Fe^{4+} (0.585 Å), in an octahedral environment. Moreover, the films present somewhat larger cell volume than the FD powders, likely due to differences in the oxygen and Fe^{3+} content, both related to the synthesis method used.

Electrode materials were deposited symmetrically on the CGO backbone to increase the TPB sites and consequently the performance, following the spray-pyrolysis procedure aforementioned. Only the results for $Sr_{0.98}Fe_{0.8}Ti_{0.2}O_{3-\delta}$ ($SFT_{0.2}$) are presented herein, because this composition exhibits the best properties to be used as symmetrical electrode. Samples with Ti-content (x>0.4) exhibit very low electronic conductivity in air to be used efficiently as electrode materials.[24,53]

Fig. S3 shows a representative Rietveld plot of the XRD pattern for $SFT_{0.2}$ treated in air. Two different cubic phases, assigned to the perovskite $SFT_{0.2}$ electrode (s.g. Pm-3m) and the fluorite CGO backbone (s.g. Fm-3m), are observed. The fit is very good and no impurity phases are detected in the studied temperature range (RT-800 ºC). It is worth noting that the chemical compatibility between $SFT_{0.2}$ and both CGO and LSGM electrolytes was confirmed in a previous work up to 1100 ºC.[20]. This sample was also annealed in humidified 5% H_2-Ar for 12 h at 750 ºC and no evidence of phase degradation was observed (Fig. S4).

Figures 2a and 2b display the SEM micrographs at the LSGM/CGO interface before the spray-pyrolysis deposition of the electrodes. The CGO layer with a thickness of 20 µm exhibits good contact with the electrolyte. This layer is porous and is comprised of connected particles of 200 nm of diameter. Figure 2c shows the LSGM/CGO interface after the deposition of $SFT_{0.2}$ by spray-pyrolysis. As can be observed the electrode is incorporated inside the porous CGO layer, reducing drastically its porosity. In fact, some regions of the electrode present low porosity due to the large amount of deposited electrode inside the CGO backbone. The amount of deposited electrode was estimated by the weigh difference before and after spray-pyrolysis deposition, resulting in a weight ratio CGO:$SFT_{0.2}$ = 0.7:0.3. SEM images at higher magnification reveal that the surface of CGO grains is completely covered with catalyst particles, ensuring a good electrical conductivity and extended TPB sites for the electrochemical reactions in the whole layer (Fig. 2d). The average grain size of $SFT_{0.2}$ coating is around 50 nm after annealing at 800 ºC. It should be commented that the use of pore formers to increase the porosity of CGO layer would result in electrodes with higher porosity and possibly better performance.

For the sake of comparison, the electrode morphology for powders, prepared by freeze-drying and deposited by screen-printing method, is displayed in Fig. S5. The grain size ~500 nm of diameter is one order of magnitude larger than that obtained by spray-pyrolysis due to the higher deposition temperature, 1100 ºC for 1 h.

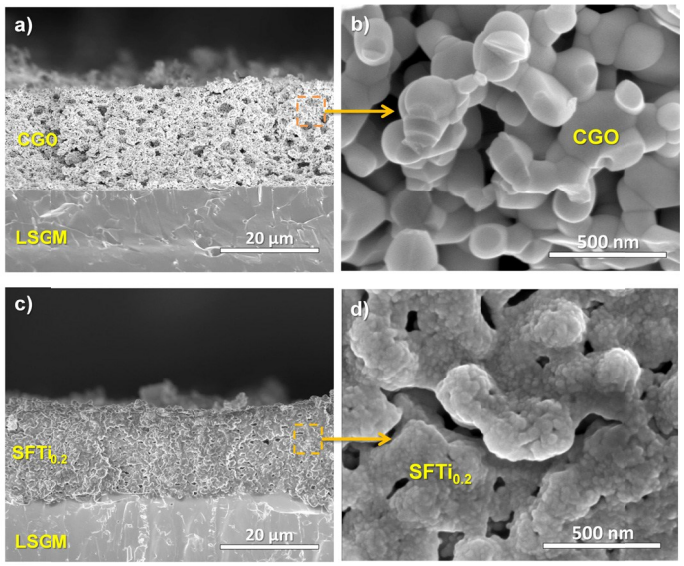

Fig. 2. SEM image at the LSGM/CGO interface (a, b) before and (c, d) after the spray-pyrolysis deposition of $Sr_{0.98}Fe_{0.8}Ti_{0.2}O_{3-\delta}$.

3.2. Electrochemical characterization of the electrodes

Impedance spectra for $SFT_{0.2}$-CGO/LSGM/$SFT_{0.2}$-CGO symmetrical cell under air and hydrogen containing atmospheres are shown in Fig. 3. As it can be observed, the electrode polarization resistance for samples prepared by spray-pyrolysis (SP) is reduced by a factor of 5 in air and by a factor of 3 in diluted hydrogen with respect to the same sample prepared by freeze-drying (FD) method. The electrode response shows similar features for both samples and atmospheres, consisting in two overlapped contributions, which are denoted as high frequency (HF) and low frequency (LF). The data were fitted to an equivalent circuit formed by (RQ) elements in series to study separately the different contributions to the electrode polarization.[27]

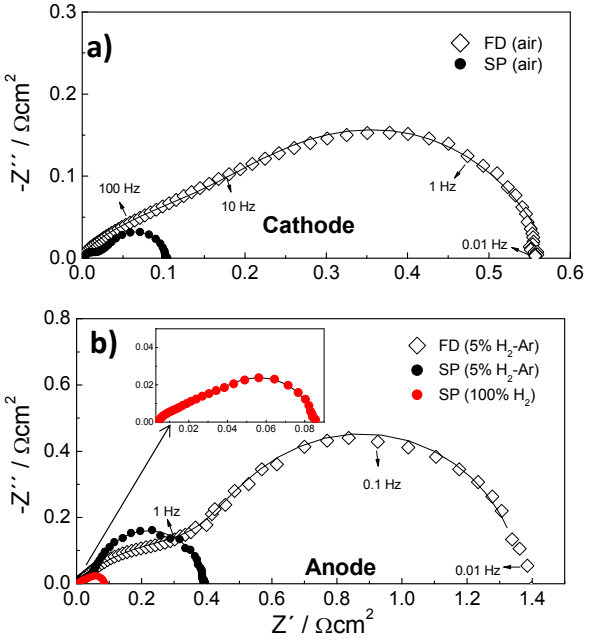

Fig. 3. Impedance spectra for $Sr_{0.98}Fe_{0.8}Ti_{0.2}O_{3-\delta}$ prepared by spray-pyrolysis (SP) and freeze-drying (FD) in (a) air and (b) H_2-containting atmospheres at 700 ºC.

In 5% H_2-Ar atmosphere, the LF response is the main contribution to the overall polarization resistance (Fig. 3b). This process appears between 0.3 and 1.5 Hz in the temperature range of 600-800 ºC and has a large capacitance value of 0.08-0.16 Fcm^2, suggesting that this contribution is possibly associated with gas diffusion limitations due to the use of diluted hydrogen. In fact, this process decreases drastically in pure H_2, further confirming this hypothesis (inset Fig. 3b). A similar behavior was observed previously for $SrTi_{1-x}Fe_xO_{3-\delta}$-CGO composite anodes, where the LF response increased strongly with decreasing hydrogen partial pressure.[39] In contrast, the HF response is less affected by the fuel concentration and appears between 100 and 300 Hz and it contains processes like charge transfer and hydrogen oxidation reaction steps.

The resistance associated with each response under oxidizing atmospheres was studied at various oxygen partial pressures (pO_2) to obtain further insights on the rate-limiting-steps involved in the oxygen reduction reactions (Fig. 4a). These resistances are usually dependent on the oxygen partial pressure: $R \propto (pO_2)^{-m}$, where the exponent *m* provides information on the type of processes involved in the cathode polarization.[54]

The LF response is the main contribution to the cathode polarization and is attributed to oxygen dissociation with m~0.5 (Fig. 4b). In contrast, the HF response is pO_2 independent, suggesting that molecular or atomic oxygen are not involved in this process. Thus, the HF contribution is assigned to charge transfer.

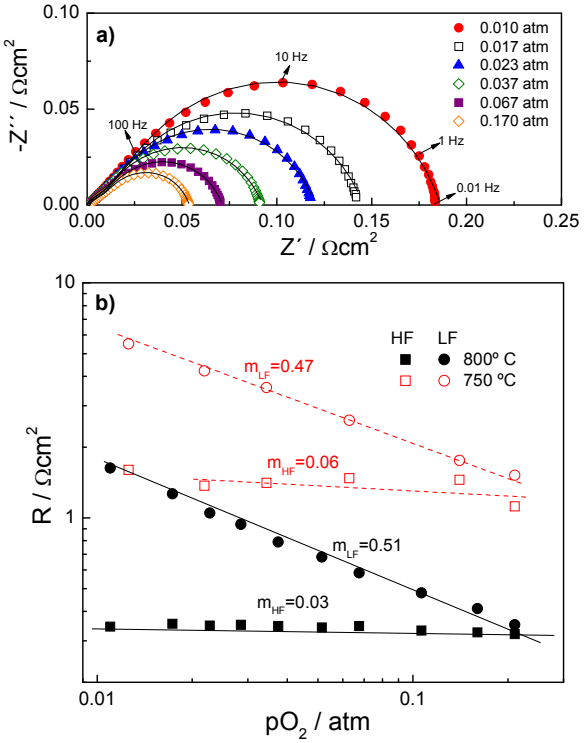

Fig. 4. a) Impedance spectra of $Sr_{0.98}Fe_{0.8}Ti_{0.2}O_{3-\delta}$ at 800 ºC and b) resistance of HF and LF contributions as a function of the oxygen partial pressure.

Overall polarization resistance R_p values are plotted in Figure 5. All the samples present a quite lineal dependence with the inverse of the temperature. The electrodes prepared by SP exhibit a R_p of 0.1 Ωcm^2 at 700 ºC in air, which is significantly lower than that obtained for FD powder samples, 0.65 Ωcm^2 (Fig. 5a). The R_p values also improve in 5% H_2-Ar, i.e. 0.35 Ωcm^2 for SP and 1.6 Ωcm^2 for FD samples at 700 ºC (Fig. 5b). Moreover, a significant decrease is observed in pure H_2, e.g. 0.07 Ωcm^2 at 700 ºC for SP sample. It should be highlighted that these are among the best R_p values reported for a symmetric electrode as summarized in Table S1.

The better performance of the nanostructured electrodes is clearly attributed to extended active sites for electrochemical reactions. On the other hand, the high ionic conductivity of CGO improves the oxygen incorporation into the lattice and the migration of the ions to the electrolyte. It should also be noted that the electronic conductivity of $SFT_{0.2}$ decreases drastically under reducing atmosphere from 40 Scm^{-1} in air to 0.5 Scm^{-1} in 5% H_2-Ar at 600 ºC due to the partial reduction $Fe^{4+} \rightarrow Fe^{3+}$ with the consequent decrease of electronic charge carriers.[24-26] Nevertheless, CGO is a mixed electronic-ionic conductor under reducing atmosphere and improves the conductivity of the anode.

The impedance spectra were acquired after consecutive oxidizing/reducing cycles between 500 and 750 ºC, obtaining reproducible results, and confirming the high stability of these materials as symmetric electrodes.

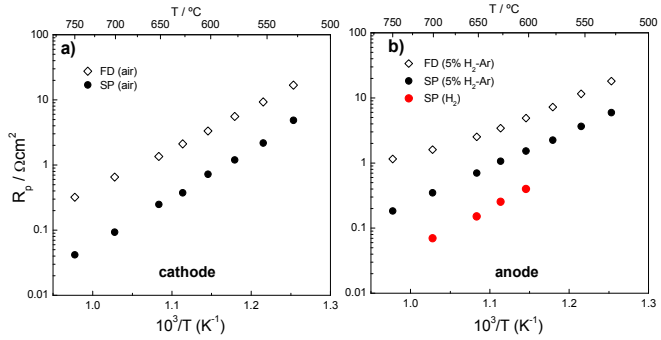

Fig. 5. Overall polarization resistances R_p for $Sr_{0.98}Fe_{0.8}Ti_{0.2}O_{3-\delta}$ prepared by spray-pyrolysis (SP) and freeze-drying (FD) in (a) air and (b) H_2-containting atmospheres.

3.3. Fuel cell test.

An electrolyte-supported cell with the following configuration $SFT_{0.2}$-CGO/LSGM/$SFTi_{0.2}$-CGO was fabricated. A cross-section micrograph of the cell after the electrochemical tests is shown in Fig. S6. The electrolyte with a thickness of 300 µm is completely dense and the symmetrical electrodes are well adhered to the electrolyte without the presence of delaminations or cracks. In addition, the nanometric particle size of SFT0.2 coating is retained after oxidation/reduction cycles, confirming the good microstructural stability of these electrodes at temperatures below 800 ºC.

Current-voltage and power density curves, using static air as oxidant and humidified H_2 as fuel, are shown in Figure 6a. The open circuit voltage is close to the Nernst potential (OCV=1.1 V). The maximum power densities are 700 and 140 $mWcm^{-2}$ at 800 and 600 ºC, respectively. These values are relatively high compared to the state-of-the-art materials (Table S1). For instance, the symmetric electrodes $La_{0.75}Sr_{0.25}Cr_{0.5}Mn_{0.5}O_{3-\delta}$ and $Sr_2Fe_{1.5}Mo_{0.5}O_{6-\delta}$ showed power density values of 550 $mWcm^{-2}$ at 950 ºC and 500 $mWcm^{-2}$ at 800 ºC, respectively.[4,9]

The ohmic losses, R_s, about 0.32, 0.41 and 0.56 Ωcm^2 at 800, 750 and 700 ºC, respectively, are in good agreement with those estimated for a 300 µm thick LSGM electrolyte (Fig. 6b). In addition, the values of polarization resistance, 0.09, 0.15 and 0.28 Ωcm^2 at 800, 750 and 700 ºC, respectively are lower than the corresponding ohmic losses, indicating that the fuel cell efficiency is mainly limited by the thick electrolyte. Thus, the fuel cell performance might be improved by reducing the electrolyte thickness.

Finally, the fuel cell stability was studied for 48 h at 750 ºC and no evidence of degradation was observed, confirming that these nanostructured electrodes are stable at intermediate temperatures.

4. CONCLUSIONS

$Sr_{0.98}Fe_{1-x}Ti_xO_{3-\delta}$ films were prepared by a simple method based on spray-pyrolysis deposition of an aqueous cation solution of metal nitrates and EDTA. Single crystalline phases with cubic perovskite structure were obtained in the compositional range $0 \le x \le 0.8$. These materials were also deposited on porous CGO layers at sufficiently low temperature to allow their incorporation inside the backbone. As a result an electrode coating layer was formed in the whole surface of CGO grains, providing a higher catalytic area for the electrochemical reactions. These electrodes were prepared in only one deposition-thermal step, simplifying the electrode fabrication with respect to the classical wet-infiltration.

$Sr_{0.98}Fe_{0.8}Ti_{0.2}O_{3-\delta}$ nanostructured electrode was found to be stable under oxidizing and reducing conditions up to 800 ºC and showed polarization resistance values at 750 ºC of 0.04 and 0.18 Ωcm^2 in air and 5% H_2-Ar, respectively, compared to 0.32 and 1.15 Ωcm^2 for submicrometric powders obtained from freeze-dried precursors.

Power densities of 700 and 140 $mWcm^{-2}$ at 800 and 600 ºC were obtained for a 300 µm thick LSGM electrolyte-supported cell with $Sr_{0.98}Fe_{0.8}Ti_{0.2}O_{3-\delta}$ symmetric electrodes, using static air as oxidant and humidified hydrogen as fuel. The values of power density were limited by the thick LSGM electrolyte with ohmic and polarization losses of 0.41 and 0.15 Ωcm^2, respectively, at 750 ºC.

$Sr_{0.98}Fe_{0.8}Ti_{0.2}O_{3-\delta}$ showed high performance at relatively low temperature with LSGM electrolyte, in comparison to most of the symmetrical electrodes previously reported; and is expected to operate efficiently with other electrolytes, such as those based on doped ceria at intermediate temperatures.

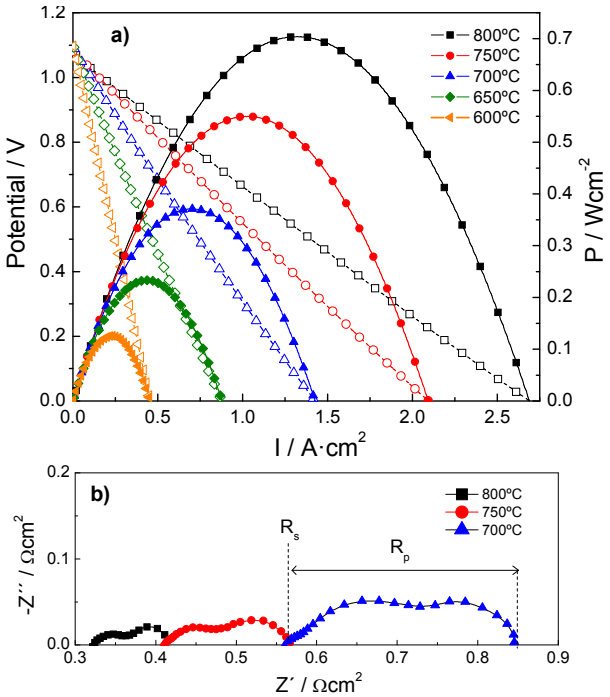

Fig. 6. (a) I–V and power density curves for a symmetric cell with LSGM electrolyte and $Sr_{0.98}Fe_{0.8}Ti_{0.2}O_{3-\delta}$ symmetric electrodes, (b) impedance spectra of the cells at various temperatures.

Acknowledgements

This work was supported by the MAT2013-41836-R grant (Spain). L. dos Santos-Gómez thanks to the Spanish Ministry of Education, Culture and Sports for her predoctoral fellowships (FPU). We are grateful to David Manteca for his help in the preparation of the materials.

Notes and references

1 E. D. Wachsman, K. T. Lee, *Science*, 2011, **334**, 935.
2 S. C. Singhal, K. Kendall, High Temperature Solid Oxide Fuel Cells: Fundamental, Design and applications, Elservier, Oxford, 2004.

3 D. M. Bastidas, S. W. Tao, J. T. S. Irvine, *J. Mater. Chem*., 2006, **16**, 1603.
4 J. C. Ruíz-Morales, J. Canales-Vázquez, J. Peña-Martínez, D. Marrero-López, P. Núñez, *Electrochim. Acta*, 2006, **52**, 278.
5 J. C. Ruíz-Morales, D. Marrero-López, J. Canales-Vázquez, J. T. S. Irvine, *RSC Adv*., 2011, **1**, 1403.
6 C. Su, W. Wang , M. Liu, M. O. Tadé, Z. Shao, *Adv. Energy Mater.*, 2015, **5**, 1500188.
7 B. Lin, S. L. Wang, X. Q. Liu, G. Y. Meng, *J. Alloys Compd*., 2010, **490**, 214.
8 Y. Zheng, C. Zhang, R. Ran, R. Cai, Z. Shao, D. Farrusseng, *Acta Materialia*, 2009, **57**, 1165.
9 Q. Liu, X. H. Dong, G. L. Xiao, F. Zhao, F. L. Chen, *Adv. Mater*., 2010, **22**, 5478.
10 J. Canales-Vázquez, J. C. Ruíz-Morales, D. Marrero-López, J. Peña-Martínez, P. Núñez, P. Gómez-Romero, *J. Power Sources*, 2007, **171**, 552.
11 R. Martínez-Coronado, A. Aguadero, D. Pérez-Coll, L. Troncoso, J. A. Alonso, M. T. Fernández-Díaz, *Int. J. Hydrogen Energy*, 2012, **37**, 18310.
12 Y. Song, Q. Zhong, W. Y. Tan, C. Pan, *Electrochim. Acta*, 2014, **139**, 13.
13 X. Liu, D. Han, Y. Zhou, X. Meng, H. Wu, J. Li, F. Zeng, Z. Zhan, *J. Power Sources*, 2014, **246**, 457.
14 Y. Zhang, Q. Zhou, T. He, *J. Power Sources*, 2011, **196**, 76.
15 J. Zhou, G. Chen, K. Wu, Y. Cheng, *J. Power Sources*, 2014, **270**, 418.
16 A. Aguadero, D. Pérez-Coll, J. A. Alonso, S. J. Skinner, J. Kilner, *Chem. Mater*., 2012, **24**, 2655.
17 Z. B. Yang, N. Xu, M. F. Han, F. L. Chen, *Int. J. Hydrogen Energy*, 2014, **39**, 7402.
18 B.-K. Lai, K. Kerman, S. Ramanathan, *J. Power Sources*, 2011, **196**, 1826.
19 G. Yang, J. Shen, Y. Chen, M. O. Tadé, Z. Shao, *J. Power Sources*, 2015, **298**, 184.
20 G. M. Yang, C. Su, R. Ran, M. O. Tadé, Z. P. Zhao, *Energy Fuels*, 2013, **28**, 356.
21 P. Zhang, G. Guan, D. S. Khaerudini, X. Hao, C. Xue, M. Han, Y. Kasai, A. Abudula, *J. Power Sources*, 2015, **276**, 347.
22. J. Lu, Y-M. Yin, J. Li, L. Xu, Z-F. Ma, *Electrochem. Commun*., 2015, **61**, 18.
23 J. M. Porras-Vázquez, T. Pike, C. A. Hancock, J. F. Marco, F. J. Berry, P. R. Slater, *J. Mater. Chem. A*, 2013, **1**, 11834.
24 A. J. Fernández-Ropero, J. M. Porras-Vázquez, A. Cabeza, P. R. Slater, D. Marrero-López, E. R. Losilla, *J. Power Sources*, 2014, **249**, 405.
25 A. A. Markov, M. V. Patrakeev, O. A. Savinskaya, A. P. Nemudry, I. A. Leonidov, O. N. Leonidova, V. L. Kozhevnikov, *Solid State Ionics*, 2008, **179**, 99.
26 V. V. Kharton, A. P. Viskup, A. V. Kovalevsky, J. R. Jurado, E. N. Naumovich, A. A. Vecher, J. R. Frade, *Solid State Ionics*, 2000, **133**, 57.
27 L. dos Santos-Gómez, J. M. Compana, S. Bruque, E. R. Losilla, D. Marrero-López, *J. Power Sources*, 2015, **279**, 419.
28 D. Ding, X. Li, S. Lai, K. Gerdes, M. Liu, *Energy Environ. Sci*., 2014, **7**, 552.
29 Y. Huang, J. M. Vohs, R. J. Gorte, John Wiley & Sons, Inc., 2006, 179, Hoboken, NJ, USA.
30 X. Zhu, Z. Lu, B. Wei, X. Huang, Y. Zhang, W. Su, *J. Power Sources*, 2011, **196**, 729.
31 X. Meng, X. Liu, D. Han, H. Wu, J. Li, Z. Zhan, *J. Power Sources*, 2014, **252**, 58.
32 A. Princivalle, D. Perednis, R. Neagu, E. Djurado, *Chem. Mater.,* 2004, **16**, 3733.
33 J. Im, I. Park, D. Shin, *Solid State Ionics,* 2011, **192**, 448.
34 D. Marrero-López, L. dos Santos-Gómez, J. Canales-Vázquez, F. Martín, J. R. Ramos-Barrado, *Electrochim. Acta*, 2014, **134**, 159.
35 N. I. Karageorgakis, A. Heel, A. Bieberle-Hütter, J. L. M. Rupp, T. Graule, L. J. Gauckler, *J. Power Sources,* 2010, **195**, 8152.
36 D. Marinha, L. Dessemond, J. S. Cronin, J. R. Wilson, S. A. Barnett, E. Djurado, *Chem. Mater.,* 2011, **23**, 5340.
37 P. L. B. Silva, R. P. Vieira, C. M. Halmenschlager, F. F. Oliveira, C. P. Bergmann, *Ceram. Int.l,* 2015, **41**, 13304.
38 A. P. Jamale, S. U. Dubal, S. P. Patil, C. H. Bhosale, L. D. Jadhav, *Appl. Surf. Sci.*, 2013, **286**, 78.
39 I. Taniguchi, R. C. van Landschoot, J. Schoonman, *Solid State Ionics,* 2003, **156**, 1.
40 C.-L. Chang, C.-S. Hsu, B.-H. Hwang, *J. Power Sources*, 2008, **179**, 734.
41 R. K. Sharma, M. Burriel, E. Djurado, *J. Mater. Chem. A*, 2015, **3**, 23833.
42 U. P. Muecke, K. Akiba, A. Infortuna, T. Salkus, N. V. Stus, L. J. Gauckler, *Solid State Ionics,* 2008, **178**, 1762.
43 Liu, G. Y. Kim, A. Chandra, *J. Power Sources,* 2012, **210**, 129.
44 L. dos Santos-Gómez, E. R. Losilla, F. Martín, J. R. Ramos-Barrado, D. Marrero-López, *ACS Appl. Mater. Inter*., 2015, **7**, 7197.
45 D. Marrero-López, M. C. Martín-Sedeño, J. Peña-Martínez, J. C. Ruíz-Morales, P. Núñez, J. R. Ramos-Barrado, *J. Am.. Ceram. Soc*., 2011, **94**, 1031.
46 X´Pert HighScore Plus Program, Version 3.0e, PANalytical B.V., Amelo, The Netherlands, 2012.
47 A. C. Larson and R. B. V. Dreele, General Structure Analysis System (GSAS) program. Los Alamos National Lab. Rep. No. LA-UR-86748, 1994.
48 D. Johnson, ZView: Asoftware Program for IES Analysis, Version 2.8, Scribner Associates, Inc., Southern Pines, NC, 2002.
49 Y. Chen, W. Jung, Z. Cai, J. Jin Kim, H. L. Tuller, B. Yildiz, *Energy Environ. Sci*., 2012, **5**, 7979.
50 J. Mizusaki, M. Okayasu, S. Yamauchi, K. Fueki, *J. Solid State Chem*., 1992, **99**, 166.
51 J. P. Hodges, S. Short, J. D. Jorgensen, X. Xiong, B. Dabrowski, S. M. Mini, C. W. Kimball, *J. Solid State Chem*., 2000, **151**, 190.
52 S. Cho, D. E. Fowler, E. C. Miller, J. S. Cronin, K. R. Poeppelmeier, S. A. Barnett, *Energy Environ. Sci*., 2013, **6**, 1850.
53 P. I. Cowin, R. Lan, C. T. G. Petit, S. Tao, *Solid State Sci*., 2015, **46**, 62.
54 E. Siebert, A. Hammouche, M. Kleitz, *Electrochim. Acta*, 1995, **40**, 1741.

Graphical Abstract

Ti-doped $SrFeO_{3-\delta}$ electrodes, prepared by a novel method based on spray-pyrolysis deposition, exhibit high efficiency as both cathode and anode in SOFCs.